Direct measurement of foldover in cavity magnon-polariton systems

P. Hyde,[1] B. M. Yao,[1,2,3,*] Y. S. Gui,[1] Guo-Qiang Zhang,[4] J. Q. You,[4,5] and C.-M. Hu[1,†]

[1]*Department of Physics and Astronomy, University of Manitoba, Winnipeg, Canada R3T 2N2*

[2]*State Key Laboratory of Infrared Physics, Shanghai Institute of Technical Physics, Chinese Academy of Sciences, Shanghai 200083, People's Republic of China*

[3]*Nantong Academy of Intelligent Sensing, Shanghai Institute of Technical Physics, Chinese Academy of Sciences, Nantong 226000, People's Republic of China*

[4]*Quantum physics and Quantum Information Division, Beijing Computational Science Research Center, Beijing 100193, People's Republic of China*

[5]*Department of Physics, Zhejiang University, Hangzhou 310027, People's Republic of China*

(Received 21 September 2018; revised manuscript received 27 October 2018; published 19 November 2018)

An approach to directly measure the nonlinear foldover effect for cavity magnon polaritons is demonstrated by placing a nonlinear medium (yttrium iron garnet) into a Fabry-Perot-like microwave cavity. The resulting bistability features can exhibit clockwise, counterclockwise, and butterflylike hysteresis loops and are solely dependent on the relative weight of the magnonlike and photonlike components. In addition to accurately describing our experimental observations, our model also allows us to calculate the crucial system conditions required to produce photonlike foldover effects. Though the photon subsystem has no nonlinear components of its own, these photonlike foldover effects are produced through light-matter interactions with a nonlinear magnetic subsystem. Our model's description of these nonlinear light-matter interactions and their effects is not limited to ferromagnetic systems and should be generally applicable to other coherent coupled systems.

DOI: 10.1103/PhysRevB.98.174423

I. INTRODUCTION

Systems undergoing nonlinear dynamics differ dramatically from their linear counterparts. One ubiquitous example, found across mechanical [1], optical [2,3], charge dynamic [4,5], magnetic systems [6–9], and two-dimensional material [10,11] is that the system's dynamic properties will be modified in response to an applied driving force. One signature of nonlinear dynamics is that they can significantly modify the structure of resonance curves, producing amplitude dependent shifts of the resonance frequency from its "natural" value and distorting of the resonance line shape to produce a foldover effect [1,6,12–15]. These nonlinear effects impact not only our physical understanding of a system's dynamics but also have important technological implications in modern electronics [5], advanced optical devices for controlling light with light [2], novel spintronic devices in data storage [16] and microwave applications [17,18], as well as developed mechanical devices for energy harvesting [19,20].

Placing such a nonlinear medium inside a cavity, the strong coupling interactions between light and matter can produce entirely new nonlinear dynamics [21], such as enhanced cooling efficiency in cavity optomechanics [22,23]. Recently, the first magnon-polariton bistabilities have been observed by inserting a small yttrium iron garnet (YIG) sphere into a high-Q 3D microwave cavity [24]. Here the cavity magnon-polariton (CMP) is generated by the strong coupling between the magnons and cavity microwave photons [25–36]. In the nonlinear experiment presented in Ref. [24], their cavity is specially designed with a third port connected to a loop antenna in the vicinity of the YIG sphere which efficiently drives the magnon mode. They also found that optical bistabilities can be achieved through light-matter interactions with bistable magnetic systems. This observation indicates that CMPs can serve as a bridge or transducer between optical and magnetic bistabilities, introducing new techniques for using one effect to manipulate and control the other.

Inspired by this new discovery, we created a nonlinear CMP system by placing a highly polished YIG sphere in the center of a Fabry-Perot-like cavity [36]. In our experiment a high power microwave generator drives the cavity subsystem, and the fields produced by the cavity resonance mode are then used to excite resonance in the YIG. At high input power this excites the coupled CMP system to nonlinear regimes, whose dynamics can then be detected with a spectrum analyzer. This implementation allows us to use the same frequency for the driving and probing fields and to perform an in-tune two-port measurement. From our measurements, we found that distinct bistability features appear among magnonlike, photonlike, and mixed CMP states, each of which can be explained by our model. While the rich array of CMP bistability features is beyond what can be seen in uncoupled magnon systems during foldover, the power dependence of the critical foldover values is the same for both coupled and uncoupled systems, as seen in our model and experimental observations. This model indicates that the coupling strength and damping of the cavity should be carefully designed in order to produce foldover effects for photonlike CMPs.

*yaobimu@mail.sitp.ac.cn
†Can-Ming.Hu@umanitoba.ca

II. THEORETICAL MODEL

To derive the dynamics of nonlinear foldover in a strongly coupled magnon-photon system, we start with a model Hamiltonian [24] that explicitly takes into account both the nonlinear Kerr effect of the magnon excitation and the strong interaction between the cavity microwave photons and the magnons in a YIG sphere (in reduced units with $\hbar \equiv 1$):

$$H = \omega_c a^\dagger a + \omega_m b^\dagger b + K b^\dagger b b^\dagger b + g(a^\dagger b + a b^\dagger) + \Omega(a^\dagger e^{-i\omega t} + a e^{i\omega t}). \quad (1)$$

Here $a^\dagger$ (a) and $b^\dagger$ (b) are the creation (annihilation) operators of the cavity photon at ω_c and of the magnon at ω_m, respectively. K is the Kerr coefficient of the magnon mode and g is the coupling strength between the cavity photon and the magnon. The last term in the above equation describes the oscillating external drive field with amplitude $\Omega = S\sqrt{P}$ and frequency ω, where P is input microwave power. S is a coefficient that describes the conversion between input power P and the field Ω driving the cavity resonance mode. The magnitude of S is frequency dependent, which is influenced by the cavity design and cable loss in measurement circuit.

Since the dissipation function Q can be classically defined as:

$$Q = \frac{da^\dagger}{dt}\frac{da}{dt}(\beta + \beta' a^\dagger a) + \frac{db^\dagger}{dt}\frac{db}{dt}(\alpha + \alpha' b^\dagger b), \quad (2)$$

where β and α, respectively, describe the intrinsic linear damping parameters of the cavity photon and magnon, and β' and α' are the nonlinear damping parameters [9,14]. As damping within our cavity system is not expected to have a significant nonlinear component, we set $\beta' = 0$ in our further calculations.

With both Eq. (1) and Eq. (2), the nonlinear dynamics of the coupled magnon-photon system follow:

$$i\frac{da}{dt} = \frac{\partial H}{\partial a^\dagger} + \frac{\partial Q}{\partial(da^\dagger/dt)} \quad (3)$$

$$i\frac{db}{dt} = \frac{\partial H}{\partial b^\dagger} + \frac{\partial Q}{\partial(db^\dagger/dt)}. \quad (4)$$

For this coupled anharmonic oscillator system, the complete analytical solutions describing the dynamics are complicated and not always available. Thus for simplicity, we initially solve this coupled differential system by neglecting damping terms and assuming that the responses of the system have a periodic solution, with $a = A\exp(-i\omega t)$ and $b = B\exp(-i\omega t)$, where A and B are the complex amplitudes of the cavity and the magnon mode, respectively. Reinserting this periodic solution into Eqs. (3) and (4), now including both linear and nonlinear damping terms, we find the stationary solution satisfies:

$$A = \frac{-\Omega}{\omega_c - \omega - i\beta\omega - \dfrac{g^2}{\omega_m - \omega + 2K|B|^2 - i\omega(\alpha + \alpha'|B|^2)}}, \quad (5)$$

$$B = \frac{g\Omega}{(\omega_c - \omega - i\beta\omega)[\omega_m - \omega + 2K|B|^2 - i\omega(\alpha + \alpha'|B|^2)] - g^2}. \quad (6)$$

Equations (5) and (6) look similar to those for linear CMP dynamics if we assume $\omega_m + 2K|B|^2 = \omega_m'$ and $\alpha + \alpha'|B|^2 = \alpha_m$; however for a sufficiently large Ω qualitatively different dynamic properties appear. Using Eq. (6) and its complex conjugate expression, one can obtain a cubic equation of $|B|^2$ expressed as:

$$p_0 + p_1|B|^2 + p_2|B|^4 + p_3|B|^6 = 0. \quad (7)$$

This is the frequency response equation of the Duffing equation (which describes an oscillator with cubic nonlinearity [37,38]) using harmonic balance. All coefficients of Eq. (7) are real and can be expressed as $p_0 = -\eta\Omega^2$, $p_1 = [\omega_m - \omega - \eta(\omega_c - \omega)]^2 + \omega^2(\alpha + \eta\beta)^2$, $p_2 = 4K[\omega_m - \omega - \eta(\omega_c - \omega)] + 2\alpha'\omega^2[\alpha + \eta\beta]$, and $p_3 = 4K^2 + (\alpha'\omega)^2$. Here the parameter η is defined as:

$$\eta = \frac{g^2}{(\omega_c - \omega)^2 + \beta^2\omega^2}. \quad (8)$$

The parameter η characterizes the transfer efficiency of the excitation energy into the magnon system, which is determined by the coupling strength g, frequency detuning $\omega_c - \omega$, and the damping parameter β of the cavity. While the parameter η does not change the fundamental foldover behavior of the anharmonic oscillator, as experimentally demonstrated in the next section, it provides a way to manipulate the line shape of the foldover effect through varying the frequency detuning $\omega_c - \omega$, resulting in several distinguishable bistable behaviors in the coupled system.

The real roots of Eq. (7) give the oscillation amplitude of the magnon in the coupled system. When Ω exceeds a critical value of Ω_t there is a range of frequencies where $|B|^2$ has three real roots. This range corresponds to the bistable range seen in foldover resonance [1] and is a signature of the anharmonic oscillator. The borders of this range are determined by the condition $d|B|/d(\omega - \omega_m) = \infty$. Differentiating Eq. (7) with respect to $\omega - \omega_m$, one can obtain a quadratic equation of $|B|^2$ as $p_1 + 2p_2|B|^2 + 3p_3|B|^4 = 0$, allowing the borders of the bistable state to be deduced for the case when $\Omega \gg \Omega_t$. Assuming α' is small and hence neglecting the higher order α' term, the upper and lower foldover borders are described by:

$$\omega - \omega_m = 3\sqrt[3]{\frac{2K\eta\Omega^2}{4 + (\alpha'\omega/2K)^2}} + \eta(\omega - \omega_c), \quad (9)$$

and

$$-\left[\alpha\omega + \eta\beta\omega - \frac{\alpha'\omega}{2K}(\omega_m - \omega - \eta(\omega_c - \omega))\right]^2 \times (\omega_m - \omega - \eta(\omega_c - \omega)) = 2K\eta\Omega^2. \quad (10)$$

The Ω dependence of Eq. (10) is seen to be dependent on the value of $\omega_m - \omega - \eta(\omega_c - \omega)$. In our coupled nonlinear CMP system this value represents the shift of the magnon resonance mode due to linear and nonlinear effects. For low drive powers the magnon frequency shift will be small, and the nonlinear damping term of Eq. (10) can be ignored. Conversely, at high drive powers the $\omega_m - \omega - \eta(\omega_c - \omega)$ term will become dominant and the linear damping terms in Eq. (10) can be approximated as relatively small. Thus the foldover upper border described in Eq. (10) will have very different dependences on input power Ω depending on whether the nonlinear damping (dependent on the driving field Ω) is dominant.

$$\omega - \omega_m \approx \frac{2K\eta\Omega^2}{(\alpha\omega + \eta\beta\omega)^2} + \eta(\omega - \omega_c), \text{ (small } \Omega) \quad (11)$$

$$\omega - \omega_m \approx \sqrt[3]{2K\eta\Omega^2\left(\frac{2K}{\alpha'\omega}\right)^2} + \eta(\omega - \omega_c). \text{ (large } \Omega) \quad (12)$$

The critical drive field Ω_t corresponds to the double root $\omega - \omega_m = \sqrt{3}\text{sign}(K)(\alpha\omega + \eta\beta\omega) + \eta(\omega - \omega_c)$ of the quadratic equation, where the borders of the bistable state are equivalent, and is thus (assuming small Ω and small α'):

$$\Omega_t^2 \approx \frac{4\sqrt{3}}{9|K|}\frac{[\alpha\omega + \eta\beta\omega]^3}{\eta}. \quad (13)$$

At relatively low drive fields, Eqs. (9) and (11) can be distinguished by their different field (Ω) and hence power ($P = \Omega^2/S^2$) dependences, with Eq. (9) having $\omega - \omega_m \propto P^{1/3}$ and Eq. (11) having $\omega - \omega_m \propto P$. These dependencies are exactly the same as those seen in uncoupled anharmonic oscillators and are typical of results produced by a nonlinear restoring force [14]. This difference disappears as the drive field becomes stronger and the nonlinear damping terms in Eq. (11) become dominant, eventually leading to $\omega - \omega_m \propto P^{1/3}$ for both foldover limits at very high Ω values.

At the resonance condition $\omega = \omega_c$ a large η value (large g and/or small β), will produce two effects in the CMP system, (a) an enhanced driving field for magnon precession, due to increased energy transfer from the photon subsystem to the magnon subsystem, and (b) enhanced magnon damping, due to additional energy losses from the magnon subsystem during coupling to the photon subsystem. The competition between these effects results in a minimum critical microwave power $P_t(\propto \Omega_t^2)$ required in order to observe foldover effects in CMPs. For the calculations in Fig. 1, we use a typical damping parameter $\alpha = 1 \times 10^{-4}$ for the YIG sphere and vary both β and g within their typical ranges. In Fig. 1(a), the calculated results at $\omega = \omega_c$ clearly show the conditions where P_t is minimized (white dotted line), this relation can be deduced from Eq. (13) and is described by $g = \sqrt{\alpha\beta/2}\omega$. For strong coupling, where $g^2 \gg \alpha\beta\omega_c^2$, the critical microwave power P_t is proportional to g^4/β at $\omega = \omega_c$. This indicates that coupling strength plays a crucial role in generating CMP foldover effects, especially near $\omega = \omega_c$, and moreover that high-Q cavities are not always optimal for producing foldover effects in coupled CMP systems.

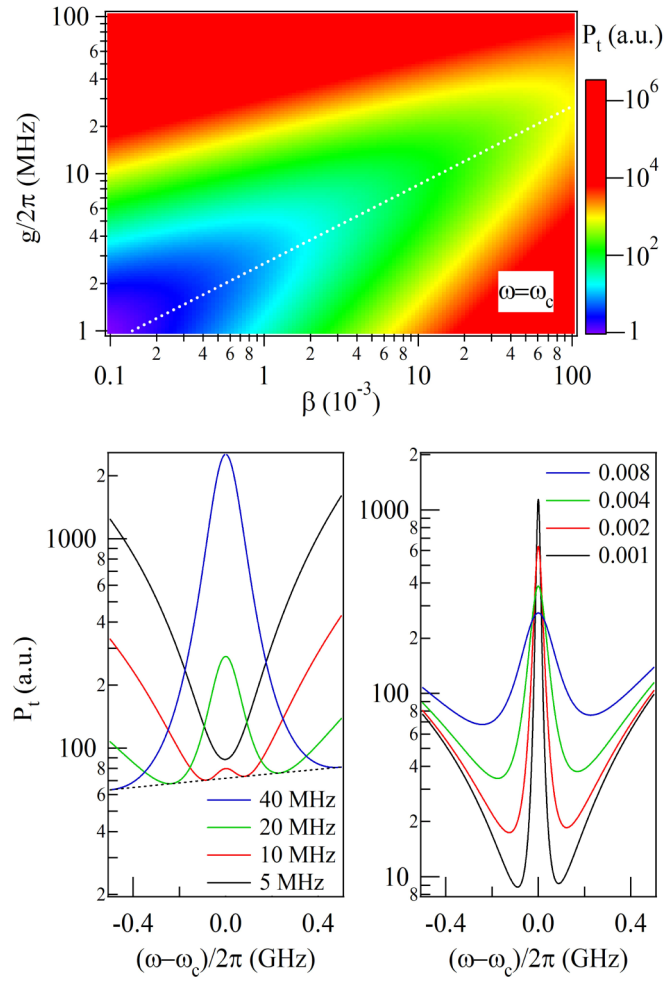

FIG. 1. (a) The critical microwave power ($P_t \propto \Omega_t^2$) required for observation of the foldover effect, calculated as a function of the coupling strength g and the damping parameter β of the cavity. The dotted line indicates the lower limit of P_t versus β. (b) P_t as a function of the frequency detuning $\omega - \omega_c$ for several g at $\beta = 0.008$. The dotted line indicates the lower limit of P_t. (c) P_t as a function of the frequency detuning $\omega - \omega_c$ for several β at $g/2\pi = 20$ MHz. In all calculations P_t is rescaled by it lowest value in (a) for $\omega_c/2\pi = 12$ GHz and $\alpha = 1 \times 10^{-4}$.

Far from the resonance condition at $\omega = \omega_c$, the lower limit of P_t occurs at $\eta(\omega, g) = \alpha/2\beta$ corresponding to $\Omega_t^2|K| = 3\sqrt{3}\alpha^2\beta\omega^3$; this is plotted (dotted line) in Fig. 1(b) as a function of the frequency detuning $\omega - \omega_c$. For small $g/2\pi$(=5 MHz) the $\alpha\omega$ term dominates in Eq. (13) and as a consequence P_t shows a minimum at $\omega = \omega_c$ due to the effective energy transfer between systems at this resonance condition. In contrast, at larger $g/2\pi$(=20 and 40 MHz) the dominant term in Eq. (13) becomes $\eta\beta\omega$ and a pronounced peak in P_t appears at $\omega = \omega_c$, due to enhanced damping near this frequency.

In Fig. 1(c), P_t versus $\omega - \omega_c$ is plotted for several β values, using $g/2\pi = 20$ MHz. Here it is clearly seen that a lower β value results in a larger P_t for on-resonance conditions but will produce a smaller P_t away from resonance. This contrast

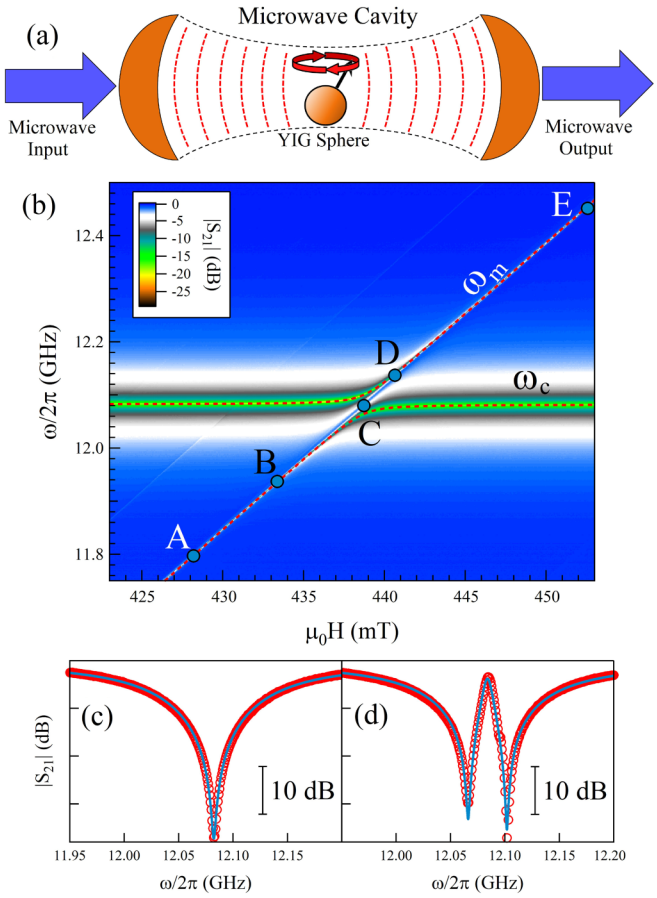

FIG. 2. (a) Schematic diagram of the experimental setup, where a YIG sphere is placed in the center of the midplane of a waveguide assembly cavity, and a static magnetic field is applied along the [110] direction of the YIG sphere. The dynamics of this coupled system are measured using the microwave transmission through this setup. (b) Transmission mapping of the hybridized CMP system, demonstrating level repulsion, with solid lines indicating the calculated CMP dispersion. Fixed field cuts (symbols) made (c) far below and (d) at the coupling point, $\omega_m = \omega_c$, with solid lines being calculations for each field based on Eq. (14).

between on and off resonance behavior is generally valid for any coupled system in the nonlinear range.

III. EXPERIMENTAL RESULTS AND DISCUSSION

The experimental setup of our measurement system is schematically shown in Fig. 2. The microwave cavity used in this work is a Fabry-Perot-like cavity based on the Ku band (12–18 GHz) assembled waveguide apparatus, where circular waveguides are connected through circular-rectangular transitions to coaxial-rectangular adapters, and the two transitions are rotated by an angle of 45°. A detailed discussion of this waveguide setup can be found in Ref. [36]. A 1 mm diameter highly-polished YIG sphere was placed in the center of the midplane of this quasi-one-dimensional cavity. During measurements a static magnetic field H was applied along the [110] direction of the YIG crystal.

The wave propagation in this ferrite loaded cavity under a magnetic bias has been analytically solved in the linear range [36]. We generalize the deduced transmission coefficient S_{21} in the nonlinear range as

$$S_{21} \propto 1 - \frac{\xi}{i(\omega_c - \omega) + \beta\omega + \frac{g^2}{i(\omega_m - \omega + 2K|B|^2) + \omega(\alpha + \alpha'|B|^2)}}. \tag{14}$$

Here the amplitude of the magnon mode $|B|$ can be calculated according to Eq. (6). As this equation is based on an approximation of $\omega \approx \omega_c$, in order to explain features far away from this resonance condition, we introduce a fitting parameter ξ, which can be deduced from the low power measurement.

The physical reason for using this kind of cavity to study nonlinear behaviors is due to its low input/output losses between the microwave ports and the cavity system. This allows higher microwave energies to be sent into the CMP system, permitting foldover effects to be seen both near to and far from cavity resonance. As will be demonstrated in Sec. III B the nonlinear behaviors of the CMP system are dependent on $\omega_c - \omega$, thus measurements of bistability effects over a wide range of frequencies are necessary to understand the full dynamics of nonlinear CMP systems.

A. Characterization of the coupled magnon and cavity mode in the linear range

We first characterize the photon-magnon system using a vector network analyzer in linear conditions, so that the contribution of $2K|B|^2$ is negligible. For our cavity resonance we use the h mode (where the microwave magnetic field is maximum at the midplane of our cavity) at $\omega_c/2\pi = 12.082$ GHz. The ferromagnetic resonance frequency of the YIG sample in our experiments follows the dispersion $\omega_m = \gamma(H_r + H_A)$, where $\gamma/2\pi = 26.9$ μ_0GHz/T is the gyromagnetic ratio, $\mu_0 H_A = 10.4$ mT is the anisotropy field, and H_r is the biased static magnetic field at resonance. The standard level repulsion of the hybridized modes was measured and is shown in Fig. 2(b). Using $g/2\pi = 18.0$ MHz, determined by the separated gap at $\omega_m = \omega_c$ in Fig. 2(d), the calculated dispersion (solid line) agrees very well with the measured data.

As the damping parameters play an important role in nonlinear foldover effects, we have deduced them from measurements taken at $\mu_0 H = 398.8$ mT, where $|\omega_c - \omega_m| \gg g$ and coupling effects are negligible. As shown in Fig. 2(c) the line shape of the cavity resonance can be well fitted using Eq. (14) by setting $\beta = 8.4 \times 10^{-3}$ and $\xi/2\pi = 99$ MHz. Similarly, we also deduce $\alpha = 1.1 \times 10^{-4}$ for the YIG sphere far from ω_c. Using these values we calculate the microwave transmission according to Eq. (14) at $\mu_0 H = 438.8$ mT (corresponding to $\omega_m = \omega_c$) using $\xi/2\pi = 99$ MHz. This calculation reproduces the measurement results at a strongly coupled condition, as shown in Fig. 2(d).

B. Bistability of magnonlike and photonlike CMPs

In this section, we present and compare nonlinear effects in our coupled magnon-cavity system for on-resonance and far off-resonance frequencies. Here high microwave powers provided by a microwave generator are used to drive the large angle precession of the magnon, while the

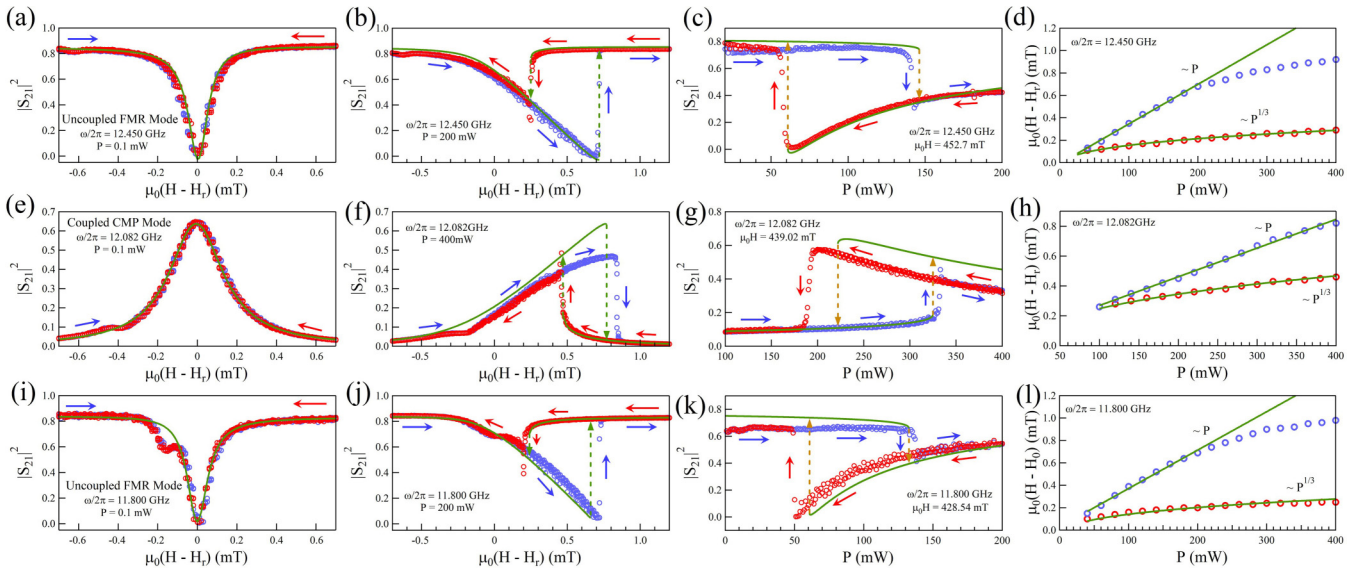

FIG. 3. (a)–(d) $\omega/2\pi = 12.450$ GHz. $|S_{21}|^2$ versus H at (a) $P = 0.1$ mW and (b) $P = 200$ mW. (c) $|S_{21}|^2$ versus P at $\mu_0 H = 452.7$ mT. (d) The jump position versus P. (e)–(h) $\omega/2\pi = \omega_c/2\pi = 12.082$ GHz. $|S_{21}|^2$ versus H at (e) $P = 0.1$ mW and (f) $P = 400$ mW. (g) $|S_{21}|^2$ versus P at $\mu_0 H = 439.025$ mT. (h) The jump position versus P. (i)–(l) $\omega/2\pi = 11.800$ GHz. $|S_{21}|^2$ versus H at (i) $P = 0.1$ mW and (j) $P = 200$ mW. (k) $|S_{21}|^2$ versus P at $\mu_0 H = 428.54$ mT. (l) The jump position versus P. Blue (red) symbols are experimental results of forward (backward) H field scans. The solid curves in (a)–(c), (e)–(g), and (i)–(k) are theoretical results calculated using Eq. (14). Dashed lines indicate the jumping positions. The solid curves in (d), (h), and (l) are theoretical results fitted using Eqs. (9) and (10) for forward and backward scans, respectively.

transmission signal is measured using a signal analyzer. We start our measurements in the linear range by setting the output power of the microwave generator to be 0.1 mW. Fixing the microwave frequency at $\omega/2\pi = 12.450$ GHz, 12.082 GHz, and 11.800 GHz, the transmission coefficients $|S_{21}|^2$ were measured as a function of the biased static magnetic field H as shown in Figs. 3(a), 3(e) and 3(i), respectively. At conditions A ($\omega/2\pi = 11.800$ GHz) and E ($\omega/2\pi = 12.450$ GHz), where the CMP is magnon dominated, the spectra show a minimum transmission at the resonance condition ($H = H_r$) because of strong absorption due to the magnon excitation. In contrast, the spectrum shows a maximum transmission at condition C ($\omega = \omega_c$). This is due to the nature of the our Fabry-Perot-like microwave resonator, where the microwaves will be more effectively absorbed by the cavity near $\omega = \omega_c$ than at off-resonance conditions [36]. Strongly coupling this cavity to a YIG magnon mode at $\omega = \omega_c$ will thus result in a maximum transmission signal at $H = H_r$, with only a single transmission peak visible due to the fact that only the YIG subsystem is influenced by changes to H [39].

Additionally, the linewidth of the peak at $\omega = \omega_c$ is seen to be significantly larger, with measured linewidths of 1.6 MHz (0.06 mT), 4.5 MHz (0.17 mT), and 1.7 MHz (0.06 mT) at $\omega/2\pi = 12.450$ GHz, 12.082 GHz, and 11.800 GHz, respectively. This effect can be explained as an effective damping of $\alpha\omega + \eta\beta\omega$ in coupled magnon-cavity systems. The higher damping near $\omega = \omega_c$ is related to the redistribution of microwave density of states within the cavity [35]. We can further calculate the line shape of the resonance (solid lines) according to Eq. (14) by adjusting $\xi/2\pi = 180$ MHz, 89 MHz, and 175 MHz for $\omega/2\pi = 12.450$ GHz, 12.082 GHz, and 11.800 GHz, respectively. Comparisons between the measurement results (symbols) and calculations (lines) are shown in Figs. 3(a), 3(e) and 3(i). An additional feature on the low-field side of the resonance corresponds to a high order magnon mode and has been studied in detail elsewhere, in both linear [24] and nonlinear [40] power ranges; it is not of immediate interest for our line shape discussion of nonlinear CMP foldover effects.

Increasing the microwave power, the resonance gradually shifts toward higher H because the Kerr term is negative for a [110] magnetized YIG sphere [24]. At sufficiently high powers the foldover effect appears, and Eq. (7) has three solutions, two of them stable and an additional unstable mode. In the experimental data, two abrupt jumps occur at different static magnetic H field biases and correspond to abrupt transitions between these two stable states. As a result, a hysteresis loop is clearly seen in the up- and down-sweep traces shown in Figs. 3(b), 3(f) and 3(j). The difference of the transmission amplitudes between two stable states as well as the inner area of the hysteresis loop will increase with microwave power.

Because of the difference in the implementation of experimental setup when compared with the previous report [24], the bistable behaviors are seen to be very different between magnonlike and photonlike CMPs in our magnon-cavity system [41]. When $|\omega - \omega_c| \gg g$ the field hysteresis loops for magnonlike CMPs [Figs. 3(b) and 3(j)] are counterclockwise, when considering the up- and down-sweep direction of the static magnetic field. However, at $\omega = \omega_c$ the field hysteresis loop for the photonlike CMP in Fig. 3(f) is clockwise. The power hysteresis loops, which measure the transmission at fixed ω and H as microwave power P is swept, also demonstrate this difference. We find the power hysteresis loops for magnonlike CMPs in Figs. 3(c) and 3(k) to be clockwise, when considering the direction of increasing and decreasing microwave power sweeps, and the power hysteresis loop for

the photonlike CMP at $\omega = \omega_c$ in Fig. 3(g) to be counterclockwise.

In order to quantitatively model the above experimental observations, we require the values of S and K. Although these parameters cannot be determined individually in present experiments, the product parameter KS^2 can be determined by the H field jump positions according to Eqs. (9) and (10). Figures 3(d), 3(h) and 3(i) show the jump positions as a function of the microwave power at $\omega/2\pi = 12.450$ GHz, 12.082 GHz, and 11.800 GHz, respectively. As expected the up-sweep jump (symbols) follows a linear P dependence (solid line) and the down-sweep jump (symbols) follows a $P^{1/3}$ dependence (solid line), with $KS^2 = 5.77 \times 10^{-8}$, 3.75×10^{-8}, and 1.58×10^{-8} GHz^3/mW for 12.450, 12.082, and 11.800 GHz, respectively. The disagreement between experimental data and linear fittings for the up-swept jumps at high powers is a result of the nonlinear damping terms in Eq. (10) becoming larger as power is increased, and the power dependence of the jump point moving towards the $\omega - \omega_m \propto P^{1/3}$ described in Eq. 12, similar to the results found in uncoupled ferromagnetic systems described by Ref. [14].

The parameter KS^2 was deduced according to Eq. (11), where the linear damping term is dominant and a linear power dependence for the up-swept jumps is found. Then we can simulate the CMP bistability using Eq. (14) in this power range by assuming $\alpha' = 0$, which reproduces the experimental observations in Fig. 3. From this agreement, the validation of our generalized model describing CMP foldover effects in this quasi-one-dimensional cavity is clearly seen. Two stable states with different transmissions can be switched between by sweeping either the static magnetic field or the microwave power. In regards to how the number of CMPs present in the system changes during the transition, the dynamics of photonlike and magnonlike CMPs are exactly opposite.

C. Butterflylike CMP hysteresis loops

In addition to the foldover behaviors seen at on-resonance ($\omega = \omega_c$) and far-from-resonance ($|\omega - \omega_c| \gg g$) conditions, a distinctly different CMP foldover hysteresis loop is seen at intermediate frequencies above and below ω_c. In Sec. III B we saw that at low microwave powers the microwave transmission line shape $|S_{21}(H)|^2$ of CMPs have a typical Lorentzian peak characteristic at $\omega = \omega_c$ and a Lorentzian dip characteristic for $|\omega - \omega_c| \gg g$. However, in general $|S_{21}(H)|^2$ will have an asymmetric lineshape [42] in the linear range, with the polarity of this asymmetry reversing as ω crosses ω_c. This asymmetric line shape observed by sweeping the applied field at fixed frequency is described as Fano-like resonance [42].

We first perform measurements at an intermediate frequency below ω_c ($\omega/2\pi = 11.938$ GHz) in the linear range by setting the output microwave power of the microwave generator to be 0.1 mW. As shown in Fig. 4(a), the field swept line shape is asymmetric with a dip at the right side of H_r. As microwave power is increased, the resonant structure is observed to shift to higher fields. When this shift is sufficiently large a sharp jump appears, whose position is determined by the field sweep direction. Although the positions of these up and down sweep jumps (experimental data not shown) have power dependences described by Eqs. (9) and (10), the same

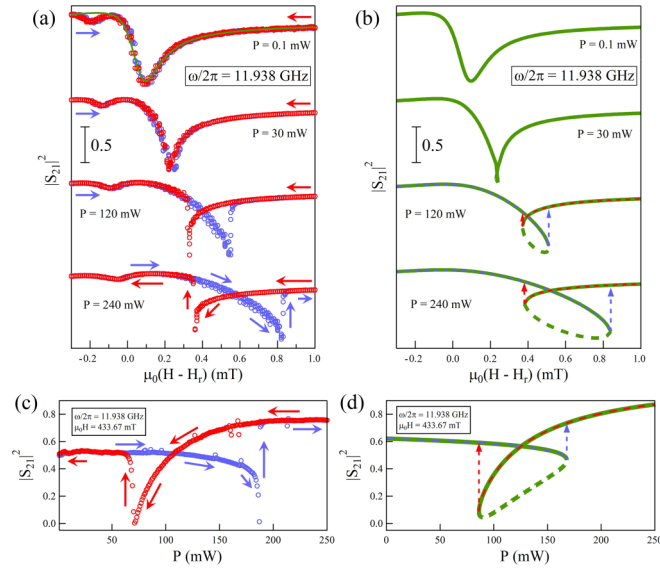

FIG. 4. Microwave $|S_{21}(H)|^2$ transmission measurements below ω_c ($\omega/2\pi = 11.938$ GHz). (a) Field swept transmissions measured at increasing microwave powers. The line over the lowest power measurement is a fitting result to Eq. (14) used to determine ξ, which was then used to calculate the S_{21} spectra at higher powers shown in (b). (c) and (d) show the measured and calculated power swept hysteresis loops at $\mu_0 H = 433.67$ mT.

power dependences as seen in the measurements discussed in Sec. III B, these jumps are seen to produce distinctly different field swept hysteresis loops. In Sec. III B the hysteresis loops observed can be described as either clockwise or counterclockwise, because one jump corresponds to the transition from a small number to a large number of CMPs within the coupled system, while the other jump corresponds to the reverse transition. However, at the intermediate frequency shown in Fig. 4(a) both jumps correspond to the transition from a small to large number of CMPs, resulting in a butterflylike hysteresis loop.

The measured data at low power ($P = 0.1$ mW) can be well fitted by Eq. (14) with $\xi/2\pi = 107$ MHz as shown in Fig. 4, where the symbols are experimental data and solid lines are fitting results. The parameter $KS^2 = 2.3 \times 10^{-8}$ GHz^3/mW was deduced from the power dependent jump positions according to Eqs. (9) and (10). For a clearer comparison, particularly at higher powers, we plotted the calculated results in Fig. 4(b), where the unstable mode is indicated by a dotted line. These calculated results show that the butterflylike hysteresis loops we measure are the result of nonlinear foldover at intermediate frequencies near ω_c. We can further compare the measured [Fig. 4(c)] and calculated [Fig. 4(d)] hysteresis loops for our power sweep results. Here we again see a butterflylike loop, which can be accurately described by our model. These butterflylike hysteresis features we have described show a bistable behavior that is not found in previous studies of either magnetic [14] or coupled magnon-cavity [24] systems.

Interestingly, the polarity of the butterflylike hysteresis loop changes if the microwave frequency is set at intermediate frequencies above ω_c. Setting $\omega/2\pi = 12.136$ GHz and

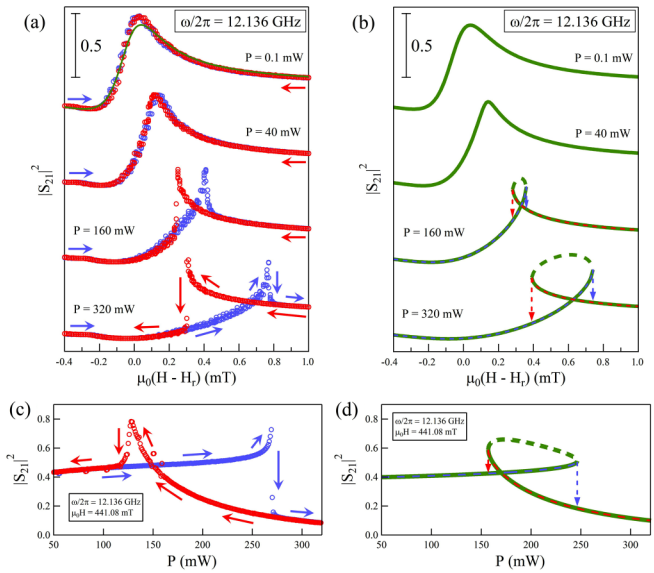

FIG. 5. Microwave $|S_{21}(H)|^2$ transmission measurements above ω_c ($\omega/2\pi = 12.136$ GHz). (a) Field swept transmissions measured at increasing microwave powers. The line over the lowest power measurement is a fitting result to Eq. (14) used to determine ξ, which was then used to calculate the S_{21} spectra at higher powers shown in (b). (c) and (d) show the measured and calculated power swept hysteresis loops at $\mu_0 H = 441.08$ mT.

measuring at low microwave power we find the field swept line shape is again asymmetric but with a maximum on the right side of H_r. The experimental data (symbols) can be well fitted (solid lines) by Eq. (14) using $\xi/2\pi = 47$ MHz. The evolution of the field swept line shape is simulated in Fig. 5(b) using the deduced nonlinear parameter $KS^2 = 1.95 \times 10^{-8}$ GHz^3/mW, deduced from the power dependent jump positions. At these intermediate frequencies above ω_c, butterflylike hysteresis loops can be observed and simulated for both field and power swept measurement, as shown in Fig. 5. As both observed jumps correspond to a transition from a large number to a small number of CMPs, a reversed butterflylike hysteresis loop results.

When compared with the results discussed in Sec. III B, we can conclude that observation of butterflylike bistabilities is caused by the asymmetric component of the resonance line shape, which has also shown in our model. In an uncoupled magnon system, similar bistable features can be expected to occur in ferromagnetic resonance measurements using electrical detection methods, as manipulating the relative phase of the microwave signal in these systems can produce asymmetric lineshapes similar to those seen in our system at intermediate frequencies [43]. We also believe that the butterflylike bistablity features we measure are not limited to magnon-related systems but should be observable across many areas of physics and engineering because the Fano-like resonance is a general wave phenomenon.

D. "Phase diagram" of CMP power hysteresis loops

The general features of power swept loops in a coupled magnon-cavity system are summarized in Fig. 6, where the green lines indicate the CMP dispersion. The CMPs will have

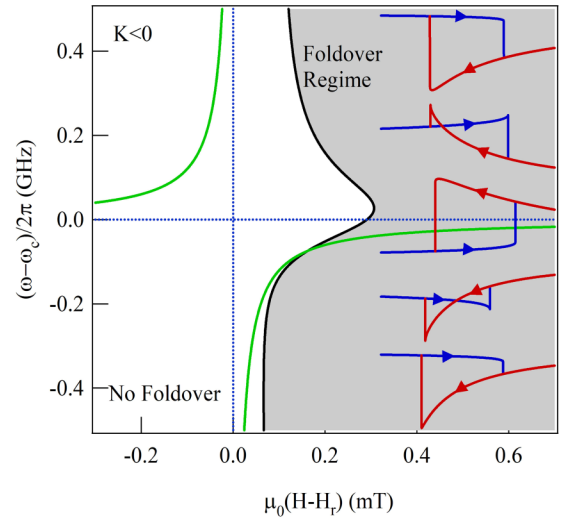

FIG. 6. "Phase diagram" of CMP power hysteresis loops of negative Kerr term, where the gray color indicates the region where CMP bistability is observed. Distinct bistable behaviors are observed: clockwise, butterflylike, counterclockwise, reversed butterflylike, and clockwise hysteresis loops appear as the measured frequency of the system is increased from far above to far below ω_c. Arrows indicate the sweeping direction of the microwave power.

more photonlike properties as their dispersion approaches $\omega = \omega_c$ (horizontal dotted line) and will take on more magnonlike properties as they approach $\omega_m = \gamma(H_r + H_A)$ (vertical dotted line). For $K < 0$ the foldover effect can only be observed in the gray area because the resonance position is shifted to higher fields as microwave power increases. The low-field border (black line) is the critical field determined by

$$H = H_r + \frac{-\sqrt{3}\,\mathrm{sign}(K)(\alpha\omega + \eta\beta\omega) + \eta(\omega - \omega_c)}{\gamma}. \quad (15)$$

This resonancelike feature is sharply different from the critical field condition of $H = H_r - \sqrt{3}\alpha\omega/\gamma$ seen in uncoupled magnetic systems [14]. The larger shift of the border toward higher H can be attributed to the enhanced damping of the magnon resonance near $\omega = \omega_c$ [35].

In contrast to previous reports studying either uncoupled magnetic systems [14] or coupled magnon-cavity systems [24], multiple bistable features are seen to exist in our coupled CMP system. As shown in Fig. 6 distinct bistable behaviors are observed: clockwise, butterflylike, counterclockwise, reversed butterflylike, and clockwise hysteresis loops as the measured frequency of the system is increased from far above to far below ω_c. These foldover features remain for $K > 0$, but in this case the foldover effects occur below H_r and the polarity of all hysteresis loops will reverse.

IV. CONCLUSIONS

In conclusion, we have theoretically and experimentally studied the foldover dynamics of CMPs in a coupled magnon-cavity system. Our carefully designed CMP system allows us to measure CMP foldover effects at frequencies below, at, and above ω_c. While many CMP foldover properties, such as H field swept jump positions, have behavior similar to those in

uncoupled magnon systems, distinct differences appear in the bistability features. We observe the power hysteresis loops to be clockwise for photonlike CMPs, counterclockwise for magnonlike CMPs, and butterflylike (reversed butterflylike) for intermediate frequencies above (below) ω_c where the CMPs have a mixed photon-magnon state.

With this multitude of available CMP bistability features, the coupled magnon-cavity system can provide a versatile platform for understanding and developing novel low-energy switching devices. Moreover, because the Fano-like resonance lineshape produced by CMP coupling is a general wave phenomenon, the nonlinear features observed in our study range may be reproducible across many areas of physics and engineering.

ACKNOWLEDGMENTS

This work was funded by NSERC, NSFC (No. 11429401 and No. 11804352), the China Scholarship Council and the Science and Technology Commission of Shanghai Municipality (STCSM No. 16ZR1445400). B.M.Y. acknowledges financial support from the Shanghai Pujiang Program (No. 18PJ1410600). G.Q.Z. and J.Q.Y. are supported by the National Key Research and Development Program of China (Grant No. 2016YFA0301200) and the National Natural Science Foundation of China (NSFC) (Grant No. 11774022). P.H. is supported by the UMGF program. We would like to thank M. Harder, M. Elyasi, Ya. M. Blanter, and Gerrit E. Bauer for discussions.

[1] L. D. Landau and E. M. Lifshitz, *Mechanics*, 2nd ed. (Pergamon Press, Oxford, 1969).
[2] H. Gibbs, *Optical Bistability: Controlling Light with Light* (Elsevier, New York, 2012).
[3] S. R. K. Rodriguez, W. Casteels, F. Storme, N. Carlon Zambon, I. Sagnes, L. Le Gratiet, E. Galopin, A. Lemaitre, A. Amo, C. Ciuti, and J. Bloch, Phys. Rev. Lett. **118**, 247402 (2017).
[4] B. Merkel, A. Kurzmann, J.-H. Schulze, A. Strittmatter, M. Geller, and A. Lorke, Phys. Rev. B **95**, 115305 (2017).
[5] S. M. Sze and K. K. Ng, *Physics of Semiconductor Devices* (John Wiley & Sons, New York, 2006).
[6] P. W. Anderson and H. Suhl, Phys. Rev. **100**, 1788 (1955).
[7] A. G. Gurevich and G. A. Melkov, *Magnetization Oscillations and Waves* (CRC, Boca Raton, FL, 1996).
[8] G. Bertotti, I. D. Mayergoyz, and C. Serpico, Phys. Rev. Lett. **87**, 217203 (2001).
[9] I. Barsukov, H. K. Lee, A. A. Jara, Y.-J. Chen, A. M. Goncalves, C. Sha, J. A. Katine, R. E. Arias, B. A. Ivanov, and I. N. Krivorotov, arXiv:1803.10925.
[10] Kelvin J. A. Ooi and Dawn T. H. Tan, Proc. R. Soc. London A **473**, 20170433 (2017).
[11] D. Davidovikj, F. Alijani, S. J. Cartamil-Bueno, H. S. J. van der Zant, M. Amabili, and P. G. Steeneken, Nat. Commun. **8**, 1253 (2017).
[12] K. D. McKinstry, C. E. Patton, and M. Kogekar, J. Appl. Phys. **58**, 925 (1985).
[13] Y. S. Gui, A. Wirthmann, N. Mecking, and C.-M. Hu, Phys. Rev. B **80**, 060402 (2009).
[14] Y. S. Gui, A. Wirthmann, and C.-M. Hu, Phys. Rev. B **80**, 184422 (2009).
[15] P. A. P. Janantha, B. Kalinikos, and M. Wu, Phys. Rev. B **95**, 064422 (2017).
[16] C. Thirion, W. Wernsdorfer, and D. Mailly, Nat. Mater. **2**, 524 (2003).
[17] S. I. Kiselev, J. C. Sankey, I. N. Krivorotov, N. C. Emley, R. J. Schoelkopf, R. A. Buhrman, and D. C. Ralph, Nature (London) **425**, 380 (2003).
[18] A. A. Tulapurkar, Y. Suzuki, A. Fukushima, H. Kubota, H. Maehara, K. Tsunekawa, D. D. Djayaprawira, N. Watanabe, and S. Yuasa, Nature (London) **438**, 339 (2005).
[19] F. Cottone, H. Vocca, and L. Gammaitoni, Phys. Rev. Lett. **102**, 080601 (2009).
[20] R. L. Harne and K. W. Wang, Smart Mater. Struct **22**, 023001 (2013).
[21] M. Aspelmeyer, T. J. Kippenberg, and F. Marquardt, Rev. Mod. Phys. **86**, 1391 (2014).
[22] S. Huang and G. S. Agarwal, Phys. Rev. A **79**, 013821 (2009).
[23] Y. C. Liu, Y. F. Xiao, X. Luan, and C. W. Wong, Phys. Rev. Lett. **110**, 153606 (2013).
[24] Y.-P. Wang, G.-Q. Zhang, D. Zhang, T.-F. Li, C.-M. Hu, and J. Q. You, Phys. Rev. Lett. **120**, 057202 (2018).
[25] Ö. O. Soykal and M. E. Flatté, Phys. Rev. Lett. **104**, 077202 (2010).
[26] Ö. O. Soykal and M. E. Flatté, Phys. Rev. B **82**, 104413 (2010).
[27] H. Huebl, C. W. Zollitsch, J. Lotze, F. Hocke, M. Greifenstein, A. Marx, R. Gross, and S. T. B. Goennenwein, Phys. Rev. Lett. **111**, 127003 (2013).
[28] Y. Tabuchi, S. Ishino, T. Ishikawa, R. Yamazaki, K. Usami, and Y. Nakamura, Phys. Rev. Lett. **113**, 083603 (2014).
[29] X. Zhang, C.-L. Zou, L. Jiang, and H. X. Tang, Phys. Rev. Lett. **113**, 156401 (2014).
[30] M. Goryachev, W. G. Farr, D. L. Creedon, Y. Fan, M. Kostylev, and M. E. Tobar, Phys. Rev. Appl. **2**, 054002 (2014).
[31] B. Bhoi, T. Cliff, I. S. Maksymov, M. Kostylev, R. Aiyar, N. Venkataramani, S. Prasad, and R. L. Stamps, J. Appl. Phys. **116**, 243906 (2014).
[32] Y. Cao, P. Yan, H. Huebl, S. T. B. Goennenwein, G. E. W. Bauer, Phys. Rev. B **91**, 094423 (2015).
[33] J. A. Haigh, N. J. Lambert, A. C. Doherty, and A. J. Ferguson, Phys. Rev. B **91**, 104410 (2015).
[34] N. J. Lambert, J. A. Haigh, and A. J. Ferguson, J. Appl. Phys. **117**, 053910 (2015).
[35] L. Bai, M. Harder, Y. P. Chen, X. Fan, J. Q. Xiao, and C.-M. Hu, Phys. Rev. Lett. **114**, 227201 (2015).
[36] B. M. Yao, Y. S. Gui, Y. Xiao, H. Guo, X. S. Chen, W. Lu, C. L. Chien, and C.-M. Hu, Phys. Rev. B **92**, 184407 (2015).
[37] J. M. T. Thompson and H. B. Stewart, *Nonlinear Dynamics and Chaos* (John Wiley & Sons, New York, 2002).
[38] I. Kovacic and M. J. Brennan, *The Duffing Equation: Nonlinear Oscillators and Their Behaviour* (John Wiley & Sons, New York, 2011).
[39] M. Harder, P. Hyde, L. Bai, C. Match, and C.-M. Hu, Phys. Rev. B **94**, 054403 (2016).

[40] H. Maier-Flaig, M. Harder, R. Gross, H. Huebl, and S. T. B. Goennenwein, Phys. Rev. B **94**, 054433 (2016).

[41] Strictly speaking, the contribution from the magnon component and photon component changes when sweeping H (hence ω_m). Near the condition of $\omega = \omega_m = \omega_c$ the CMP is half magnon and half photon and the photon component becomes dominant when $|\omega_m - \omega_c| \gg g$ at $\omega = \omega_c$. However, when fixing both H and ω, the feature of the power swept hysteresis loop in the nonlinear regime does not change with H as illustrated in Fig. 6.

[42] M. Harder, L. Bai, C. Match, J. Sirker, and C.-M. Hu, Sci. China Phys. Mech. Astron. **59**, 117511 (2016).

[43] M. Harder, Y. Gui, and C.-M. Hu, Phys. Rep. **661**, 1 (2016).